Virologica Sinica 38 (2023) 23–33

Contents lists available at ScienceDirect

Virologica Sinica

journal homepage: www.keaipublishing.com/en/journals/virologica-sinica
www.virosin.org

Research Article

Zika virus non-structural protein 4B interacts with DHCR7 to facilitate viral infection

Weijie Chen [a,b,1], Yukun Li [c,1], Xiuling Yu [a,1], Zhenwei Wang [a], Wenbiao Wang [d], Menglan Rao [a], Yongkui Li [a,b], Zhen Luo [a,b], Qiwei Zhang [a,b], Jinbiao Liu [a,b,*], Jianguo Wu [a,b,*]

[a] Guangdong Provincial Key Laboratory of Virology, Institute of Medical Microbiology, Jinan University, Guangzhou, 510632, China
[b] Foshan Institute of Medical Microbiology, Foshan, 528315, China
[c] Halison International Peace Hospital, Hebei Medical University, Hengshui, 053000, China
[d] Medical Research Center, Guangdong Provincial People's Hospital, Guangdong Academy of Medical Sciences, Guangzhou, 510080, China

ARTICLE INFO

Keywords:
7-Dehydrocholesterol reductase (DHCR7)
Interferon regulatory factor 3 (IRF3)
Interferon-beta (IFN-β)
Non-structural protein 4B (NS4B)
TANK-Binding kinase 1 (TBK1)
Zika virus (ZIKV)

ABSTRACT

Zika virus (ZIKV) evolves non-structural proteins to evade immune response and ensure efficient replication in the host cells. Cholesterol metabolic enzyme 7-dehydrocholesterol reductase (DHCR7) was recently reported to impact innate immune responses in ZIKV infection. However, the vital non-structural protein and mechanisms involved in DHCR7-mediated viral evasion are not well elucidated. In this study, we demonstrated that ZIKV infection facilitated DHCR7 expression. Notably, the upregulated DHCR7 in turn facilitated ZIKV infection and blocking DHCR7 suppressed ZIKV infection. Mechanically, ZIKV non-structural protein 4B (NS4B) interacted with DHCR7 to induce DHCR7 expression. Moreover, DHCR7 inhibited TANK-binding kinase 1 (TBK1) and interferon regulatory factor 3 (IRF3) phosphorylation, which resulted in the reduction of interferon-beta (IFN-β) and interferon-stimulated genes (ISGs) productions. Therefore, we propose that ZIKV NS4B binds to DHCR7 to repress TBK1 and IRF3 activation, which in turn inhibits IFN-β and ISGs, and thereby facilitating ZIKV evasion. This study broadens the insights on how viral non-structural proteins antagonize innate immunity to facilitate viral infection via cholesterol metabolic enzymes and intermediates.

1. Introduction

As a mosquito-borne flavivirus, Zika virus (ZIKV) was initially identified from rhesus macaque in Uganda in 1947. Underwent several outbreaks worldwide, ZIKV epidemic has become a cumulative global health threat due to the explosive expansion through mosquito route, worldwide travel of asymptomatic transporters, and sexual transmission. Most of ZIKV infections in the past epidemics were asymptomatic or mild (Wang et al., 2016), however, in the last several epidemics, ZIKV infection has led to the devastating diseases, including neurological sequelae during pregnancy (microcephaly and fetal demise) and neurological disorder (Guillain-Barré syndrome) in adults (Cao-Lormeau et al., 2016; Pierson and Diamond, 2020; Rasmussen et al., 2016). Innate immune system is the first and critical line of host immune defense against viral infection. After ZIKV infection, viral RNA was recognized by intracellular retinoic acid-inducible gene I (RIG-I) (Chazal et al., 2018; Hertzog et al., 2018; Kato et al., 2006), which initiated the downstream innate immune responses, including the TANK binding kinase 1 (TBK1) activation, the interferon regulatory factor 3 (IRF3) phosphorylation and then leading to type I interferons (IFN-I) production (Fitzgerald et al., 2003; Grant et al., 2016; Xia et al., 2018) and the expression of dozens of interferon--stimulated genes (ISGs) with various antiviral effects (Savidis et al., 2016; Schneider et al., 2014).

Host immune system produces IFNs and ISGs to restrict viral infection, however, ZIKV itself evolved a variety of escape mechanisms to ensure successfully survival and replication in the host cell, such as encoding specific non-structural (NS) proteins. ZIKV genomic RNA generates seven non-structural proteins, including NS1, NS2A, NS2B, NS3, NS4A, NS4B, and NS5 (Berthoux, 2020). ZIKV NS1 recruits host deubiquitinase USP8 to stabilize caspase-1 and attenuates type I IFN signaling to benefit ZIKV infection (Zheng et al., 2018). A mutant NS1 has been reported to bind to TBK1 and decrease the phosphorylation of TBK1, leading to reduced IFN-β production (Xia et al., 2018). ZIKV NS3 binds to and sequesters human scaffold proteins (14-3-3ε and 14-3-3η) (Riedl et al., 2019), while NS4A

* Corresponding authors.
E-mail addresses: jinbiaoliu@jnu.edu.cn (J. Liu), jwu898@jnu.edu.cn (J. Wu).
[1] Weijie Chen, Yukun Li and Xiuling Yu contributed equally to this work.

https://doi.org/10.1016/j.virs.2022.09.009
Received 8 May 2022; Accepted 26 September 2022
Available online 29 September 2022

interacts with MAVS to attenuate RIG-I- and MDA5-mediated innate immune responses (Ma et al., 2018). Notably, ZIKV NS5 binds and degrades signal transducer and activator of transcription 2 (STAT2) to attenuate type I IFN signaling (Grant et al., 2016; Kumar et al., 2016). Moreover, NS5 was also been proven to interact with RIG-I and suppress the K63-linked polyubiquitination of RIG-I, thereby repressing IFN-β production (Li et al., 2020). In addition, ZIKV NS2A, NS2B, NS4A, and NS4B have also been demonstrated to overpower IFN-β production through targeting discrete elements in the RIG-I pathway (Xia et al., 2018).

To achieve efficient replication in mammalian cells, the ZIKV also relies on the host cellular lipid metabolic components to form envelope and complete viral particle assembly (Chen et al., 2020; Leier et al., 2020). Cholesterol is one of lipid components of cell membranes and participates in multiple biological functions (Ikonen, 2008). Cellular cholesterol homeostasis is closely modulated by cholesterol synthesis, including the absorption from lipoprotein particles and release to extracellular acceptors. Virtually all mammalian cells are dependent on cholesterol metabolism (Luo et al., 2020). Accumulating evidences have indicated that cholesterol metabolism participates in innate immune response against viral infection (Blanc et al., 2013; Petersen et al., 2014; York et al., 2015). Upon viral infection, cholesterol synthesis was markedly changed and accompanied with the enhanced expression of IFN-I and ISGs in macrophages (Li et al., 2017; Liu et al., 2008; York et al., 2015). As the key enzyme in cholesterol metabolism, cholesterol-25-hydroxylase (CH25H) converts cholesterol into 25-hydroxycholesterol (25HC), which has been identified as the biological product that contributes to innate immune response against a large majority of viruses, including human immunodeficiency virus 1 (HIV-1), vesicular stomatitis virus (VSV), herpes simplex virus 1 (HSV-1), Ebola virus (EBOV), ZIKV, murine gamma herpes virus (MHV68), Rift valley fever virus (RVFV), and Russian spring-summer encephalitis virus (RSSEV) (Blanc et al., 2013; Li et al., 2017; Liu et al., 2013). Current studies are limited in investigating how cholesterol metabolic products (e.g. 25HC) could manipulate signal transduction and participate in innate immunity. To date, the enzymes or intermediates in upstream of cholesterol biosynthesis are still not well elucidated. As the vital cholesterol metabolic enzyme, 7-dehydrocholesterol reductase (DHCR7) could erase the C (7–8) double bond in the B ring of sterols and catalyze the cholesterol from 7-dehydrocholesterol (7-DHC) (Luu et al., 2015). 7-DHC is also a forerunner of vitamin D, and DHCR7 mutations links to higher vitamin D, suggesting DHCR7 displays complicatedly biological effects in conversion of cholesterol and vitamin D (Kuan et al., 2013; Prabhu et al., 2016a). A well-presented study has shown that DHCR7 silence could activate the PI3K-AKT3 pathway, leading to IRF3 Ser385 phosphorylation and promote IFN-β production to inhibit multiple viral infection *in vitro* and *in vivo* (Xiao et al., 2020). However, the understanding of DHCR7 mediated cholesterol metabolism in ZIKV NS protein mediated immune evasion is poorly defined.

Here, we elucidate a distinct mechanism that ZIKV NS4B targets on DHCR7, a key enzyme in cholesterol synthesis, to attenuate IFN-I response and facilitate ZIKV infection. We found that ZIKV infection increased DHCR7 expression. Interestingly, enhanced DHCR7 promotes ZIKV infection, while knocking down or targeting DHCR7 with inhibitor can suppress ZIKV infection. Moreover, ZIKV NS4B could bind DHCR7 and thus induce DHCR7 expression, which inhibited TBK1 and IRF3 activation and led to reduced IFN-β and ISGs productions. Therefore, we propose that ZIKV NS4B binding to DHCR7 decreases IRF3 activation, which in turn inhibits IFN-β and ISGs to facilitate ZIKV evasion. This study widens novel insights on how ZIKV non-structural protein abolishes innate immunity to facilitate viral infection through interacting with cholesterol metabolic enzyme.

2. Materials and methods

2.1. Cell lines

U251 cells were purchased from China Center for Type Culture Collection (CCTCC) (Wuhan, China). *Cercopithecus aethiops* kidney (Vero) cells, human embryonic kidney (HEK 293T) cells, human lung adenocarcinoma (A549) cells were purchased from American Tissue Culture Collection (ATCC). Cells were maintained in Dulbecco's Modified Eagle Medium (DMEM) (Gibco) supplemented with 10% fetal bovine serum (FBS) (Gibco), penicillin (100 U/mL), and streptomycin sulfate (100 μg/mL) at 37 °C and 5% CO_2. *Aedes albopictus* (C6/36) cells were cultured in Minimum Essential Medium (MEM) supplemented with 10% FBS, penicillin (100 U/mL) and streptomycin sulfate (100 μg/mL) at 28 °C with 5% CO_2.

2.2. ZIKV amplification, titration, and infection

The ZIKV isolate z16006 (GenBank accession number, KU955589.1) was cultivated in C6/36 cells, and ZIKV was aliquoted in freezing vials and stored at −80 °C. ZIKV titers were measured by plaque assay. The cells were infected with ZIKV at the indicated multiplicity of infection (MOI) for 2 h, followed by washing with phosphate buffer saline (PBS), and then cultured, harvested and examined.

2.3. Plasmids and reagents

Expression plasmid pcDNA3.1(+)-3 × Flag was used to clone individual ZIKV gene from corresponding fragments of ZIKV cDNA. To construct pGEX6p-1-NS4B, the ZIKV NS4B was sub-cloned into pGEX6p-1 vector using ClonExpress II One Step Cloning Kit (Vazyme Biotech, Nanjing, China). The cDNAs encoding human DHCR7, RIG-I, TBK1, and IRF3 cloned into pCAGGS-HA vector or pcDNA3.1 (+)-3 × Flag vector was constructed by standard molecular cloning method. The missense mutation G410S of DHCR7 was constructed using site-directed mutagenesis method. Monoclonal rabbit anti-ZIKV envelope (GTX133314) was purchased from GeneTex (Irvine, CA, USA). Rabbit polyclonal anti-DHCR7 (A8049), rabbit monoclonal anti-ISG15 (A2416), rabbit monoclonal anti-TBK1 (A3458), rabbit monoclonal anti-P-TBK1 at Ser172 (AP1026), rabbit polyclonal anti-IRF3 (A11118), anti-rabbit IgG (ac005), and anti-mouse IgG (ac011) were purchased from ABclonal Technology (Wuhan, China). Anti-mouse FITC and anti-rabbit Cy3 secondary antibodies were purchased from Abbkine (Wuhan, China). Rabbit monoclonal anti-P-IRF3 at Ser396 (29047S) and rabbit monoclonal anti-ISG56 (14769S) were purchased from Cell Signaling Technology (CST, Boston, MA, USA). Mouse monoclonal anti-Flag (F3165), rabbit monoclonal anti-HA (H6908) and mouse monoclonal anti-GAPDH (G9295) were purchased from Sigma (St Louis, MO, USA). Mouse monoclonal anti-Flavivirus group antigen antibody (MAB10216) was purchased from Millipore (Mass, USA). Lipofectamine 2000 (11668-027) and Trizol (15596018) were purchased from Invitrogen Corporation (Carlsbad, CA, USA). Poly(I:C) was purchased from InvivoGen (San Diego, CA, USA).

2.4. Plaque assay

ZIKV containing supernatant was diluted with serum-free DMEM and infected Vero cells in 12-well plate for 2 h, followed by washing with 1 mL PBS for twice. DMEM containing 2% FBS and 2% low melting point agarose were mixed well according to 1:1 volume ratio, and 1 mL mixture was added to each well. The infected cells were cultured at 37 °C with 5% CO_2 for 5–7 days. The cells fixed with 4% paraformaldehyde for 1 h and dyed with 0.5% crystal violet for 30 min. 12-well plate washed with water, and plaques were calculated.

2.5. Lentivirus production and infection

The targeting sequences of shRNAs for the human DHCR7 were as follows: sh-DHCR7-1: 5′-ATTGCCAGCACAGACGGATTT-3′, sh-DHCR7-2: 5′-CGTGATTGACTTCTTCTGGAA-3′. The pLKO.1 vector bearing a scrambled shRNA for a negative control (Sigma-Aldrich,

St. Louis, MO, USA) or the specific target sequence was transfected into HEK293T cells together with psPAX2 and pMD2.G with Lipofectamine 2000. Viral particles containing supernatants were harvested at 36 h after transfection and then centrifuged at 210×*g* for 10 min. The cell-free supernatant phase was filtrated through a 0.45 μm filter to remove the cells debris. U251 cells were infected with lentiviral particles in the presence of 8 μg/mL polybrene. After 48 h of culture, U251 cells were selected with puromycin (2 μg/mL, Sigma). The knocking down efficiency of sh-DHCR7 was determined by RT-PCR and Western blot analysis.

2.6. Western blot

Cells were lysed by RIPA buffer supplemented with protease inhibitors and phosphatase inhibitors on ice for 1 h, then centrifuged at 4 °C, 13,000×*g* for 10 min to collect the cell lysate. Protein concentration in cell lysate was measured by bicinchoninic acid (BCA) protein assay. The protein was separated by SDS-PAGE and then transferred onto polyvinyl difluoride (PVDF) membrane. The PVDF membrane was blocked with immunoblotting blocking buffer TBST (10 mmol/L Tris-HCl, pH 7.4, 0.15 mol/L NaCl, and 0.05% Tween-20) containing 5% BSA for 1 h. After washing with TBST, the membrane was incubated with primary antibodies and second antibodies, subsequently detected using Chemiluminescence imaging system (Bio-Rad).

2.7. Total cholesterol assay

The total cholesterol in cells was detected by using Tissue total cholesterol assay kit from Applygen Technologies Inc (Beijing, China). The 5 mmol/L cholesterol standard was subjected to a serial dilution with anhydrous ethanol to draw the standard curve, and the amounts of cellular total cholesterol were calculated according to the standard curves. The experiment was conducted following the procedure provided by the manufacturer.

2.8. Co-immunoprecipitation assays

HEK293T cells were transfected with the indicated plasmids. Cells were harvested and lysed with RIPA lysis buffer supplemented with protease inhibitors. After centrifugation at 18,000×*g* for 15 min at 4 °C, cell lysates were collected and immunoprecipitated by Flag-Trap Protein-G Sepharose (GE Healthcare, Milwaukee, WI, USA) for 4 h at 4 °C. The bound proteins were eluted with 2 × loading buffer and analyzed by immunoblotting.

2.9. Real-time PCR

Total RNAs were extracted from cells by using TRIzol reagent (Invitrogen Life Technologies), and cDNA was produced with M-MLV reverse transcriptase kit (Promega, Madison, WI, USA). RT-PCR was performed using SYBR RT-PCR Kits (DBI Bio-science) on the Roche LC480. Glyceraldehyde-3-phosphate dehydrogenase (GAPDH) mRNA was set as the endogenous reference to normalize the mRNAs and the gene expression levels were calculated using the $2^{-\Delta\Delta CT}$ method. The sequences of RT-PCR primers are shown in Supplementary Table S1.

2.10. Confocal microscopy

U251 cells were transfected with plasmid and cultured for 30 h, then washed three times with PBS. Cells were fixed with 4% paraformaldehyde for 15 min and permeated with PBS containing 0.1% TritonX-100 for 5 min. After washing with PBS, the cells were sealed with PBS containing 5% BSA for 30 min. Cells were washed three times with PBS and incubated with anti-HA, anti-FLAG and anti-flavivirus, then incubated with anti-mouse FITC and anti-rabbit Cy3 secondary antibodies. Cells were stained with 4′,6-Diamidino-2-phenylindole dihydrochloride (DAPI) and performed using an Olympus confocal microscope.

2.11. GST pull-down assays

The plasmids pGEX6p-1-NS4B was transfected into *Escherichia coli* (*E. coli*) strain BL21. The GST and GST-NS4B were induced by IPTG with a final concentration of 0.5 mmol/L, and the cultures were grown for an additional 6–8 h at 37 °C. And then the GST protein and GST-NS4B protein were purified from *E. coli* bacteria. The GST or GST-NS4B protein were incubated with glutathione Sepharose beads (Novagen) and washed three times with PBS. GST and GST-NS4B protein were incubated with the eukaryotic fusion protein HA-DHCR7, which were originated from plasmids encoding HA-DHCR7-expressed HEK293T cell lysates for 4 h at 4 °C. The precipitates were washed five times, boiled in 2 × SDS-loading buffer, and detected by Western blot with anti-GST and anti-HA antibodies.

2.12. HA-DHCR7 site-directed mutagenesis

Appropriate pairs of mutagenic primers (Supplementary Table S1) were synthesized and used to generate the mutated construct by PCR. HA-DHCR7 was used as the template for PrimeSTAR® HS Premix (Takara). After PCR, wild-type plasmid remaining in the PCR product was selectively digested by *Dpn*I (New England Biolabs). The digested PCR product was transfected into *E. coli* strain DH5α. Desired mutant was confirmed by Sanger sequence analysis.

2.13. Statistical analysis

All experiments were repeated at least three times with similar results. Data are expressed as mean ± standard deviation (SD). The significance of the variability was determined by Student's two-tailed unpaired *t*-test for two group or one-way ANOVA with Dunnett's multiple comparisons test or two-way ANOVA with Sidak's multiple comparisons test for multiple group comparisons using the GraphPad Prism software (version 8.0.1). A value of $P < 0.05$ was considered to be statistical significance, and $P > 0.05$ was identified as statistically nonsignificant. For all the data, the significance was presented as $^{*}P < 0.05$, $^{**}P < 0.01$ and $^{***}P < 0.001$.

3. Results

3.1. ZIKV infection induces DHCR7 expression

Accumulating evidences have demonstrated that cholesterol metabolism influences host innate immune responses against flavivirus infection, such as ZIKV and Dengue virus (DENV) (Leier et al., 2020; Randall, 2018). DHCR7 encodes an enzyme that transforms 7-DHC into cholesterol, the last step in the biosynthesis of cholesterol (Moebius et al., 1998). We first detected *DHCR7* expression upon ZIKV infection. Human astrocyte U251 was infected with ZIKV, which dose-dependently increased *DHCR7* expression at both mRNA and protein (Fig. 1A–C). To confirm the phenomenon, we next examined *DHCR7* expression in Vero cells, and found that ZIKV infection substantially induced *DHCR7* expression (Fig. 1D–F), which was consistent with the results in U251 cells.

3.2. Targeting DHCR7 elicits a critical anti-ZIKV activity

To evaluate the effects of DHCR7 against ZIKV infection, the U251 and A549 cells were transfected with HA-DHCR7 encoding plasmid

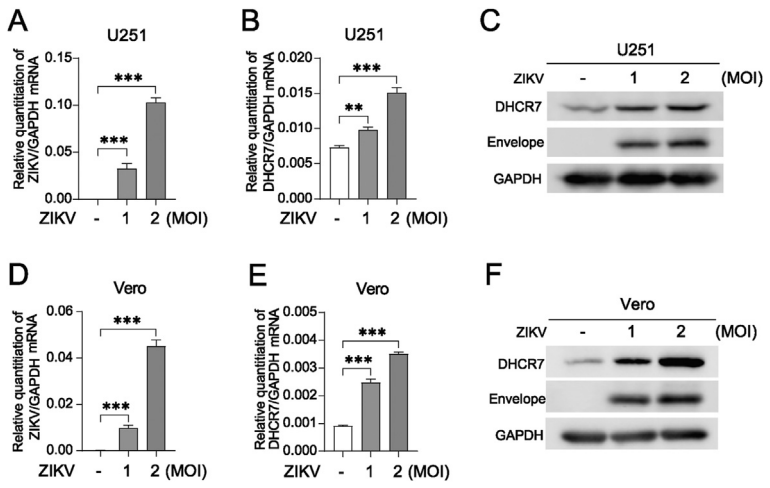

Fig. 1. ZIKV infection induces DHCR7 expression. **A–F** U251 and Vero cells were infected with ZIKV (MOI = 0, 1 and 2) for 24 h, and the intracellular RNA levels of *ZIKV* (**A, D**) and *DHCR7* (**B, E**) were determined by RT-PCR with *GAPDH* as an internal control. The relative protein levels of DHCR7 and ZIKV Envelope were detected by Western blot (**C, F**). Data are from at least three independent experiments (mean ± SD) or representative data (**C, F**). Statistical significance was calculated using one-way ANOVA with Dunnett's multiple comparisons test (**A, B, D, E**). $^{**}P < 0.01$, $^{***}P < 0.001$. SD, standard deviation.

and then infected with ZIKV (MOI = 1). The results showed that DHCR7 overexpression significantly enhanced ZIKV mRNA expression (Fig. 2A and B). Notably, with the accumulation of DHCR7 protein, the expression of ZIKV structural protein E was also increased (Fig. 2C and D). In addition, we further conducted plaque assay using the supernatant from Fig. 2C, and found that DHCR7 overexpression significantly ascended plaque forming units, as compared to control group (Fig. 2E and F). The missense mutation G410S of DHCR7 has been reported to abolish enzyme activity (Fitzky et al., 1998; Shim et al., 2004; Witsch-Baumgartner et al., 2000). To further determine the effects of DHCR7 on ZIKV infection, we next constructed inactive mutant of DHCR7 (G410S). Compared to the wild-type of DHCR7, G410S mutant could significantly inhibit ZIKV infection (Fig. 2G). We also performed confocal microscopy assay to confirm the observation. As shown in Fig. 2H, overexpression of DHCR7 increased ZIKV infection.

To determine whether endogenous DHCR7 enzyme activity is critical for ZIKV infection, we designed two short hairpin RNAs (sh-DHCR7-1 and sh-DHCR7-2) specifically targeting on DHCR7 and generated DHCR7-silenced U251 cell lines with shRNA system (Fig. 3A). Finally, we selected a sh-DHCR7-1 for its higher silencing efficiency. Compared to cell line transduced control shRNA, these DHCR7 knockdown cells showed lower susceptibility to ZIKV infection (Fig. 3B and C). We next used the selective DHCR7 inhibitor AY9944 that prevents 7-DHC conversing to cholesterol (Xu et al., 2011), which has been demonstrated to inhibit DHCR7 enzymic activity (Horlick, 1966; Moebius et al., 1998). Compared to control, AY9944 administration dose-dependently inhibited ZIKV infection in U251 cells (Fig. 3D–F). Plaque assay was also performed in Vero cells to further assess the effects of DHCR7, and showing that AY9944 could significantly suppress ZIKV infection (Fig. 3G and H). Notably, confocal microscopy showed that ZIKV E protein was substantially reduced in the presence of AY9944 (Fig. 3I). These findings indicated that targeting on DHCR7 could inhibit ZIKV infection.

3.3. DHCR7 inhibits TBK1 and IRF3 activation to reduce IFN-β and ISGs production

Since DHCR7 is the vital enzyme of converting 7-DHC to cholesterol (Moebius et al., 1998) and ZIKV infection could increase DHCR7 expression, we thus measured the cholesterol level upon ZIKV infection. We revealed that ZIKV infection has little effects on cholesterol synthesis in U251 and Vero cells (Fig. 4A and B), although DHCR7 was increased (Fig. 1A–D). Given the enhanced DHCR7 upon ZIKV infection and the key roles of IFNs in confronting ZIKV infection, we next determined the effect of DHCR7 on IFN-I signaling pathway. Control and DHCR7-silencing U251 cells were infected with ZIKV or transfected with poly(I:C), and *IFN-β* expression was explored. As compared with control group, ZIKV infection or poly(I:C) treatment markedly enhanced *IFN-β* expression in DHCR7-silencing U251 cells (Fig. 4C and D). ISGs are the effectors of interferon actions and play major roles in innate immune defense against ZIKV infection. We also demonstrated blocking DHCR7 could significantly reinforced *ISG15* and *ISG56* expression at both mRNA and protein level (Fig. 4E–J). Consistently, DHCR7 inhibitor AY9944 treatment could induce IFN-β, ISG15 and ISG56 expression (Fig. 4K, L). Importantly, the inactive mutant G410S could partially reverse the inhibitory effects of DHCR7 on IFN-β and ISGs expression (Fig. 4M, N). TBK1 and IRF3 activation is essential for IFNs-ISGs induction, thus, we next examined the effect of DHCR7 on TBK1 and IRF3 expression and activation. We demonstrated that DHCR7 not only dose-dependently inhibited the protein level, but also suppressed the level of TBK1 and IRF3 phosphorylation (Fig. 5A–C). Moreover, the inactive mutant G410S incompletely reversed the inhibitory effects of DHCR7 on IRF3 and TBK1 phosphorylation (Fig. 5D). Inconsistent with the findings of DHCR7 overexpression, AY9944 treatment could induce IRF3 and TBK1 activation in U251 cell (Fig. 5E).

3.4. ZIKV NS4B interacts with DHCR7 to inhibit TBK1 and IRF3 phosphorylation

Mounting evidence has revealed that ZIKV evolved specific NS proteins to facilitate efficient replication in host cells by directly evading host innate and adaptive immunity via a plethora of discrete mechanisms. We performed co-IP assay to screen for the individual ZIKV NS protein that could interact with DHCR7. HEK293T cells were co-transfected with pCMV-DHCR7-HA and plasmid expressing individual NS protein fused with Flag-tag. As shown in Fig. 6A, DHCR7 only binds to NS4B, but failed to interact with other NS proteins. Reciprocal co-IP assays were further conducted and showed that NS4B protein interacted with DHCR7 in HEK293T cells (Fig. 6B and C). To confirm

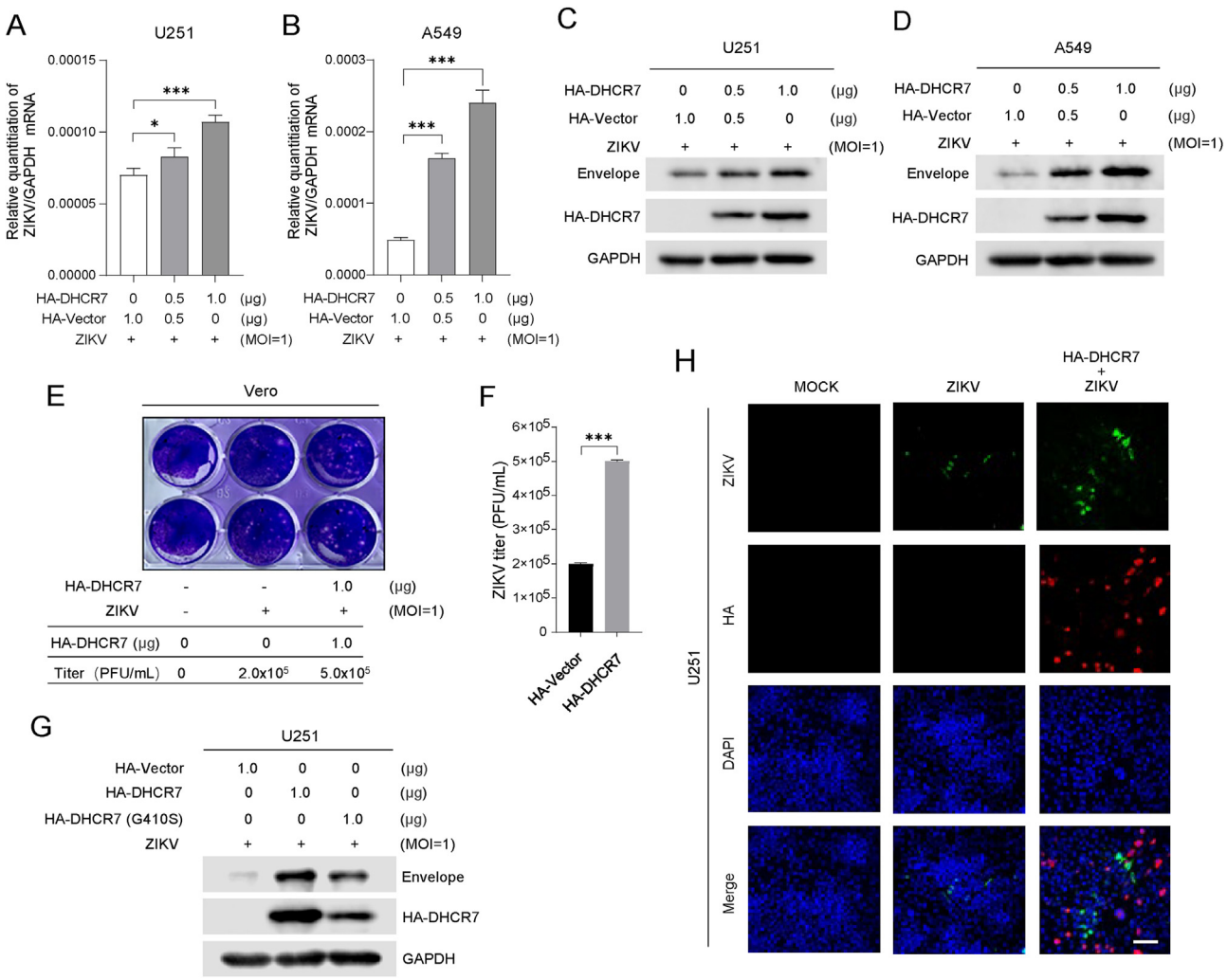

Fig. 2. Overexpression of DHCR7 promotes ZIKV replication. **A–D** U251 and A549 cells were transfected with HA-vector or HA-DHCR7 at the indicated concentrations for 12 h and then infected with ZIKV for further 36 h. The ZIKV RNA levels were detected by RT-PCR with *GAPDH* as an internal control (**A, B**), and the protein levels of ZIKV envelope, HA-DHCR7 and GAPDH were detected by Western blot (**C, D**). **E, F** Vero cells were infected with ZIKV containing supernatant from Fig. 2C for 48 h to determine ZIKV copies by plaque assay. **G** U251 cells were transfected with HA-vector, HA-DHCR7 or HA-DHCR7 (G410S) for 12 h and infected with ZIKV for 36 h, and the protein levels of ZIKV envelope, HA-DHCR7 and GAPDH were detected by Western blot. **H** U251 cells were transfected with HA-vector or HA-DHCR7 (1 μg) for 12 h and infected with ZIKV for 36 h, and subsequently incubated with mouse anti-flavivirus and rabbit anti-HA antibodies, following stained with FITC-conjugated anti-mouse and Cy3-conjugated anti-rabbit secondary antibodies. Nuclei were stained with DAPI. The images were visualized by confocal microscopy. Scale bar = 100 μm. Data are from at least three independent experiments (mean ± SD) or representative data (**C, D, E, G, H**). Statistical significance was calculated using Student's two-tailed unpaired *t*-test (**F**) or one-way ANOVA with Dunnett's multiple comparisons test (**A, B**). $^{*}P < 0.05$, $^{***}P < 0.001$. SD, standard deviation.

the interaction of NS4B and DHCR7, we next performed confocal microscope and found that NS4B protein and DHCR7 protein were co-localized in the cytoplasm (Fig. 6D). GST pull-down assay further demonstrated the interaction of NS4B and DHCR7 (Fig. 6E). Moreover, transient transfection of NS4B in U251 cells could dramatically induce DHCR7 expression (Fig. 6F). Importantly, NS4B could dose-dependently block phosphorylation of both TBK1 and IRF3, which was positively correlated with the enhanced activation of TBK1 and IRF3 in response to DHCR7 (Fig. 6G and H). However, NS4B overexpression in HEK293T cells significantly decreased protein level of TBK1, but had little effect on IRF3 protein (Fig. 6G and H). To further confirm these observations, NS4B was transfected into DHCR7 knockdown U251 cells and showed inhibitory effects on endogenous protein and phosphorylation levels of TBK1 and IRF3 (Fig. 6I). Taken together, these results demonstrated that ZIKV NS4B interacted with DHCR7 and enhanced DHCR7 expression to block TBK1 and IRF3 activation and then facilitate ZIKV infection.

4. Discussion

Type I IFNs and their downstream ISGs confront a large series of pathogens and play a crucial role in host immune defense against ZIKV (Lazear et al., 2016). To evade the IFN-mediated surveillance and achieve sufficient replication, ZIKV evolves NS proteins targeting on various points of the IFN signaling pathway to flee the cellular innate immune system (Lee et al., 2021). Mounting studies have illustrated that ZIKV NS1, NS3, NS4A, and NS5 inhibit distinct modules of the RIG-I/IFN-I pathway and facilitate viral infection utilizing independent and diverse mechanisms (Grant et al., 2016; Kumar et al., 2016; Ma et al., 2018; Riedl et al., 2019; Xia et al., 2018; Zheng et al., 2018). However, the specific mechanism of ZIKV NS4B counteracting immune restriction is poorly defined. ZIKV NS4B is an extremely hydrophobic protein consisting of 251 amino acids, and located in the endoplasmic reticulum membrane with N-terminal (Zou et al., 2014). NS4B inhibition of IFN-I signaling pathway has been identified in different flaviviruses (Ding et al., 2013;

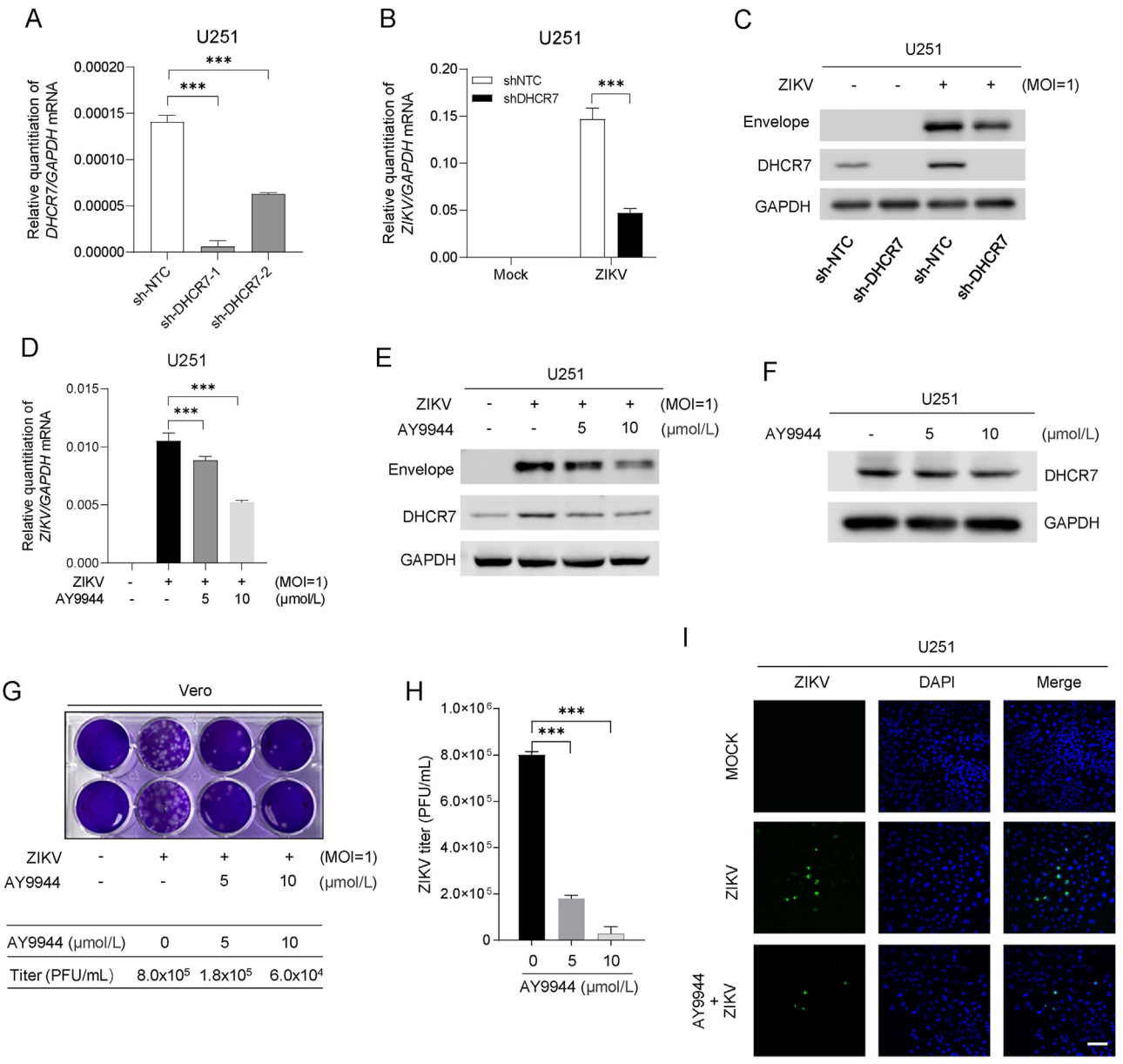

Fig. 3. Knockdown of DHCR7 reduces ZIKV infection in U251 cells. **A** U251 cells were transduced with the lentiviral particles containing shRNA against DHCR7 (sh-DHCR7-1 and sh-DHCR7-2) or a nontarget sequence (sh-NTC), followed by puromycin selection for 14 days. The knockdown efficiency was determined by RT-PCR. **B, C** DHCR7-silencing U251 (sh-DHCR7) and sh-NTC U251 cells were mock infected or ZIKV infected (MOI = 1) for 36 h. The intracellular ZIKV RNA level was detected by RT-PCR with *GAPDH* as an internal control (**B**) and the protein levels of ZIKV envelope, DHCR7 and GAPDH were detected by Western blot (**C**). **D, E** U251 cells were treated with DHCR7 inhibitor AY9944 at indicated concentration for 2 h, then infection with ZIKV (MOI = 1) for 48 h. The cells were subjected to RT-PCR to detect ZIKV RNA (**D**). The protein levels of ZIKV envelope, DHCR7 and GAPDH were detected by Western blot (**E**). **F** U251 cells were treated with DHCR7 inhibitor AY9944 at indicated concentration for 36 h, and DHCR7 and GAPDH were detected by Western blot. **G, H** Vero cells were infected with ZIKV containing supernatant from Fig. 3E for 48 h to determine ZIKV copies by plaque assay. **I** U251 cells were treated with AY9944 at indicated concentration for 2 h, then infection with ZIKV at MOI = 1 for 36 h. The images were visualized by confocal microscopy. Scale bar = 100 μm. Data are from at least three independent experiments (mean ± SD) or representative data (**C, E, F, G and I**). Statistical significance is calculated using one-way ANOVA with Dunnett's multiple comparisons test (**A, D, H**) or two-way ANOVA with Sidak's multiple comparisons test (**B**). ***$P < 0.001$. SD, standard deviation.

Munoz-Jordan et al., 2003, 2005; Shan et al., 2021; Yi et al., 2016; Zhang et al., 2021). A recent study has reported that ZIKV INMI1 strain isolated in Brazil utilizes NS4B to antagonize the downstream of IFN-I signaling pathway by crushing STAT1 phosphorylation and consequently interrupting STAT1 nuclear transport (Fanunza et al., 2021). In this study, we found a distinct mechanism that ZIKV NS4B abolished IFN-β production by suppressing TBK1 and of IRF3 phosphorylation, the upstream component of IFN-I signaling pathway. Notably, amino acid substitution (G18R) has been discovered in ZIKV NS4B, which contributed to the decreased IFN-β production and weakened ISGs expression, and consequently facilitated viral infection in mice, indicating the significance of NS4B as a determinant of pathogenesis (Gorman et al., 2018).

Emerging evidences indicated the critical importance of cholesterol metabolism participating in innate immune response (Akula et al., 2016; Dang et al., 2017; Reboldi et al., 2014; York et al., 2015). Although several intermediates in cholesterol metabolism have been documented to have broad antiviral effects (Blanc et al., 2013; Li et al., 2017; Liu et al., 2013; Xiao et al., 2020), our study illustrated a novel

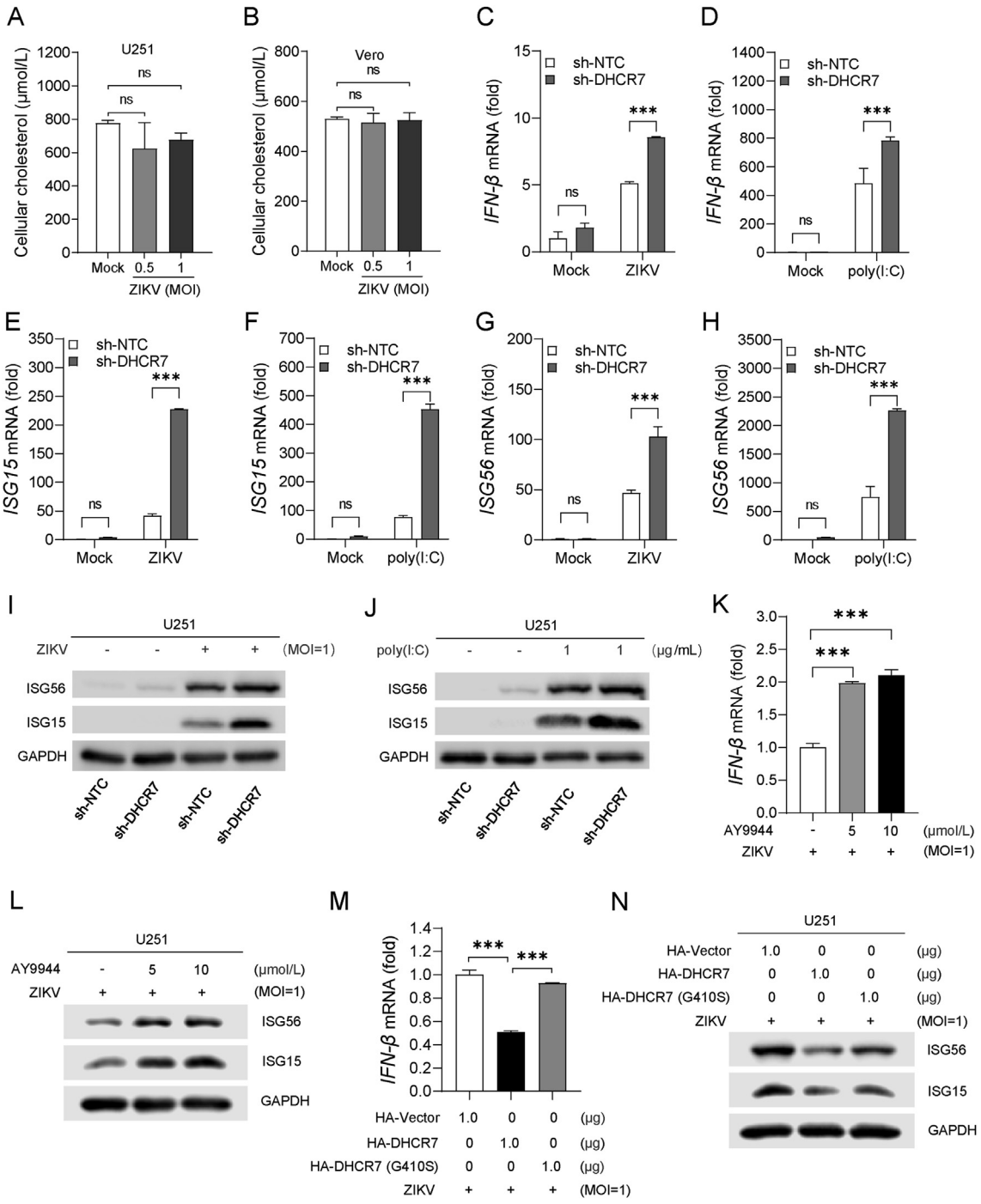

Fig. 4. DHCR7 inhibits IFN-β and ISGs production. **A, B** U251 and Vero cells were infected with ZIKV (MOI = 0, 0.5 and 1) for 24 h, and cellular cholesterol was measured by tissue total cholesterol assay kit. **C–H** DHCR7-silencing U251 (sh-DHCR7) and sh-NTC U251 cells were infected with ZIKV (MOI = 1) or treated with Poly(I:C) (1 μg/mL) for 6 h. Total cellular RNA was extracted and subjected to RT-PCR for the mRNA expression with *GAPDH* as an internal control. The relative expressions of *IFN-β* and *ISGs* were normalized to that of sh-NTC samples in mock group, and fold changes were shown in ordinate. *IFN-β* (**C, D**), *ISG15* (**E, F**) and *ISG56* (**G, H**). **I**, **J** DHCR7-silencing U251 (sh-DHCR7) and sh-NTC U251 cells were infected with ZIKV (MOI = 1) or transfected with Poly(I:C) (1 μg/mL) for 24 h, and the protein levels of ISG15, ISG56 and GAPDH were detected by Western blot. **K** U251 cells were treated with the indicated dose of AY9944 for 2 h, then infected with ZIKV (MOI = 1) for 6 h. The *IFN-β* RNA level was detected by RT-PCR with *GAPDH* as an internal control. **L** U251 cells were treated with the indicated dose of AY9944 for 2 h, and then infected with ZIKV (MOI = 1) for 24 h. The protein levels of ISG15, ISG56 and GAPDH were detected by Western blot. **M** U251 cells were transfected with HA-vector, HA-DHCR7 or HA-DHCR7 (G410S) for 24 h and infected with ZIKV (MOI = 1) for 6 h. The *IFN-β* RNA levels were detected by RT-PCR with *GAPDH* as an internal control. **N** U251 cells were transfected with HA-vector, HA-DHCR7 or HA-DHCR7 (G410S) for 24 h, and then infected with ZIKV (MOI = 1) for 24 h. The protein levels of ISG15, ISG56 and GAPDH were detected by Western blot. Data are from at least three independent experiments (mean ± SD) or representative data (**I, J, L, N**). Statistical significance is calculated using one-way ANOVA with Dunnett's multiple comparisons test (**A, B, K, M**) or two-way ANOVA with Sidak's multiple comparisons test (**C**–**H**). ns, $P > 0.05$, $^{***}P < 0.001$. SD, standard deviation.

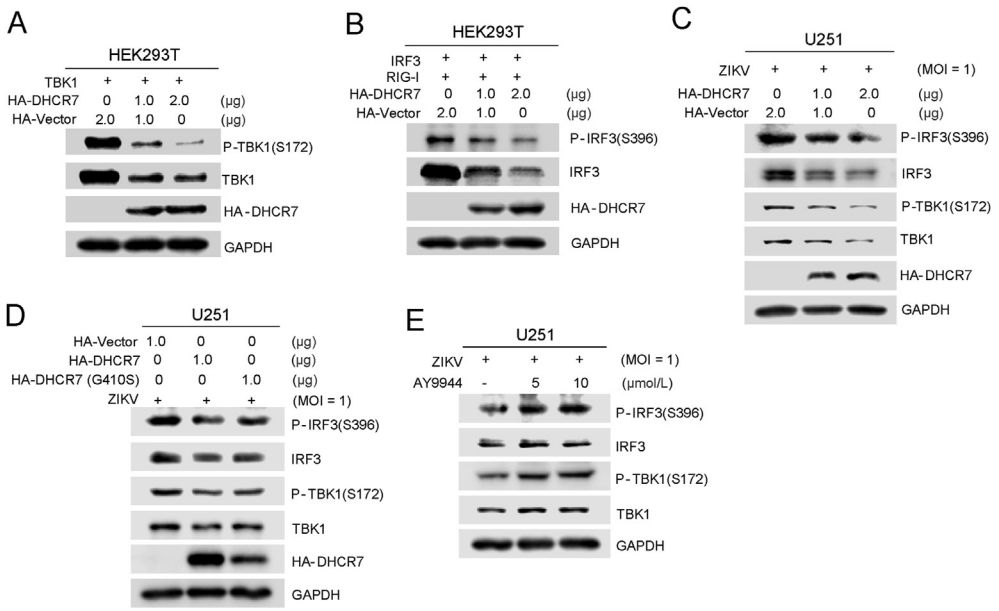

Fig. 5. DHCR7 inhibits TBK1 and IRF3 activation. **A**, **B** HEK293T cells were co-transfected with TBK1-coding plasmid together with DHCR7-expressing plasmid or empty vector (**A**). HEK293T cells were co-transfected with IRF3-ecoding plasmid, RIG-I encoding plasmid, together with DHCR7-expressing plasmid or empty vector (**B**). Cells were harvested at 24 h post-transfection and subjected to Western blot with indicated antibodies [anti-TBK1, anti-P-TBK1(S172), anti-IRF3, anti-P-IRF3(S396), anti-HA, and anti-GAPDH]. **C** U251 cells were transfected with the indicated dose of DHCR7 expressing plasmid or empty vector for 24 h. Cells were then infected with ZIKV (MOI = 1) and harvested at 6 h post-infection and subjected to Western blot with indicated antibodies [anti-TBK1, anti-P-TBK1(S172), anti-IRF3, anti-P-IRF3(S396), anti-HA, and anti-GAPDH]. **D** U251 cells were transfected with HA-vector, HA-DHCR7 or HA-DHCR7 (G410S) for 24 h. Cells were then infected with ZIKV (MOI = 1) and harvested at 6 h post-infection and subjected to Western blot with indicated antibodies [anti-TBK1, anti-P-TBK1(S172), anti-IRF3, anti-P-IRF3(S396), anti-HA, and anti-GAPDH]. **E** U251 cells were treated with the indicated dose of AY9944 for 2 h and infected with ZIKV (MOI = 1) for 6 h, then subjected to Western blot with indicated antibodies [anti-TBK1, anti-P-TBK1(S172), anti-IRF3, anti-P-IRF3(S396), and anti-GAPDH]. Data are from at least three independent experiments and shown as representative data (**A–E**).

mechanism that cholesterol metabolic enzyme DHCR7 was involved in ZIKV infection by attenuating TBK1 and IRF3 activation to facilitate viral infection. As a key enzyme involved in desmosterol and cholesterol metabolism, DHCR7 represents a switch of converting 7-DHC to vitamin D in skin cells exposed to UVB (Prabhu et al., 2016b). Moreover, DHCR7 is positioned not only at the gateway of the Bloch pathway, but also at the end of the Kandutsch-Russell pathway (Prabhu et al., 2016a, 2016b), which plays vital roles in controlling of cholesterol synthesis. The crosstalk of DHCR7 and its interaction with other enzymes in several pathways may empower multiple functions in different cell types or organs. Previous study has revealed that blocking DHCR7 could diminish desmosterol, the immediate precursor of cholesterol biosynthesis, thereby offering sufficient protection against HCV infection (Luu et al., 2015; Rodgers et al., 2012). Importantly, Xiao et al. has shown that VSV infection decreases DHCR7 expression, leading to reduced cholesterol, but much more 7-DHC accumulation in macrophages and liver (Xiao et al., 2020). Macrophages treated with 7-DHC rendered an enhanced antiviral response; while addition of cholesterol showed minor protection. The DHCR7 inhibitors and administration of 7-DHC might be useful approaches to combat viral infections such as HIN1, HSV and VSV. In this study, we found DHCR7 inhibitor AY9944 could suppress ZIKV infection. However, our study revealed that ZIKV infection induced DHCR7 expression, but had little effect on cholesterol biosynthesis in glial cells. We didn't examine the level of 7-DHC expression post ZIKV infection, nevertheless, it is worthy to further investigate whether 7-DHC and AY9944 have a synergically therapeutic efficacy to treat patients who have been infected with ZIKV infection in brain. DHCR7 overexpression promoted ZIKV infection, while the DHCR7 selective inhibitor (AY9944) treatment strongly ascended IFN-β production against ZIKV infection. TBK1 and IRF3 activation is vital for priming IFN-I signaling. Previous investigation displayed that DHCR7 silencing or 7-DHC treatment activated the PI3K-AKT3 pathway to phosphorylate IRF3, but not TBK1 in macrophages (Xiao et al., 2020). Nevertheless, our findings showed DHCR7 dose-dependently decreased both IRF3 and TBK1 expression, as well as IRF3 and TBK1 phosphorylation. These investigations suggested that DHCR7 might contribute to ZIKV infection in a cholesterol metabolism-independent mechanism in brain.

It has been well elucidated that ZIKV utilized NS proteins to directly interact with different components of RIG-I/IFN-I pathway to evade immune response and facilitate viral replication. We previously reported the interaction of ZIKV NS5 with RIG-I to attenuate IFN-β production (Li et al., 2020). Others demonstrated that ZIKV NS1 and NS2B targeted on TBK1, NS3 targeted on RIG-I and MDA5 to reduce IFN-I and ISGs production (Lee et al., 2021; Riedl et al., 2019). However, the function of ZIKV NS proteins targeting on cholesterol metabolism remains largely elusive. In this study, we have also illustrated an unreported interaction between the cholesterol metabolic enzyme DHCR7 and ZIKV NS proteins. We showed DHCR7 specifically bound to NS4B, not to other NS proteins. We provided the critical evidence that ZIKV NS4B interacted with DHCR7, and substantially induced its expression, which was consistent with results in U251 cells upon ZIKV infection. Importantly, apart from directly demonstrating the engagement of DHCR7 and ZIKV NS4B, we also found that ZIKV NS4B increased DHCR7 expression to inhibit TBK1 and IRF3 phosphorylation and facilitate ZIKV infection. In agreement with our results, recent study revealed that DHCR7 deficiency could activate IRF3 and IFN-β signaling to inhibit VSV and other viruses in macrophages.

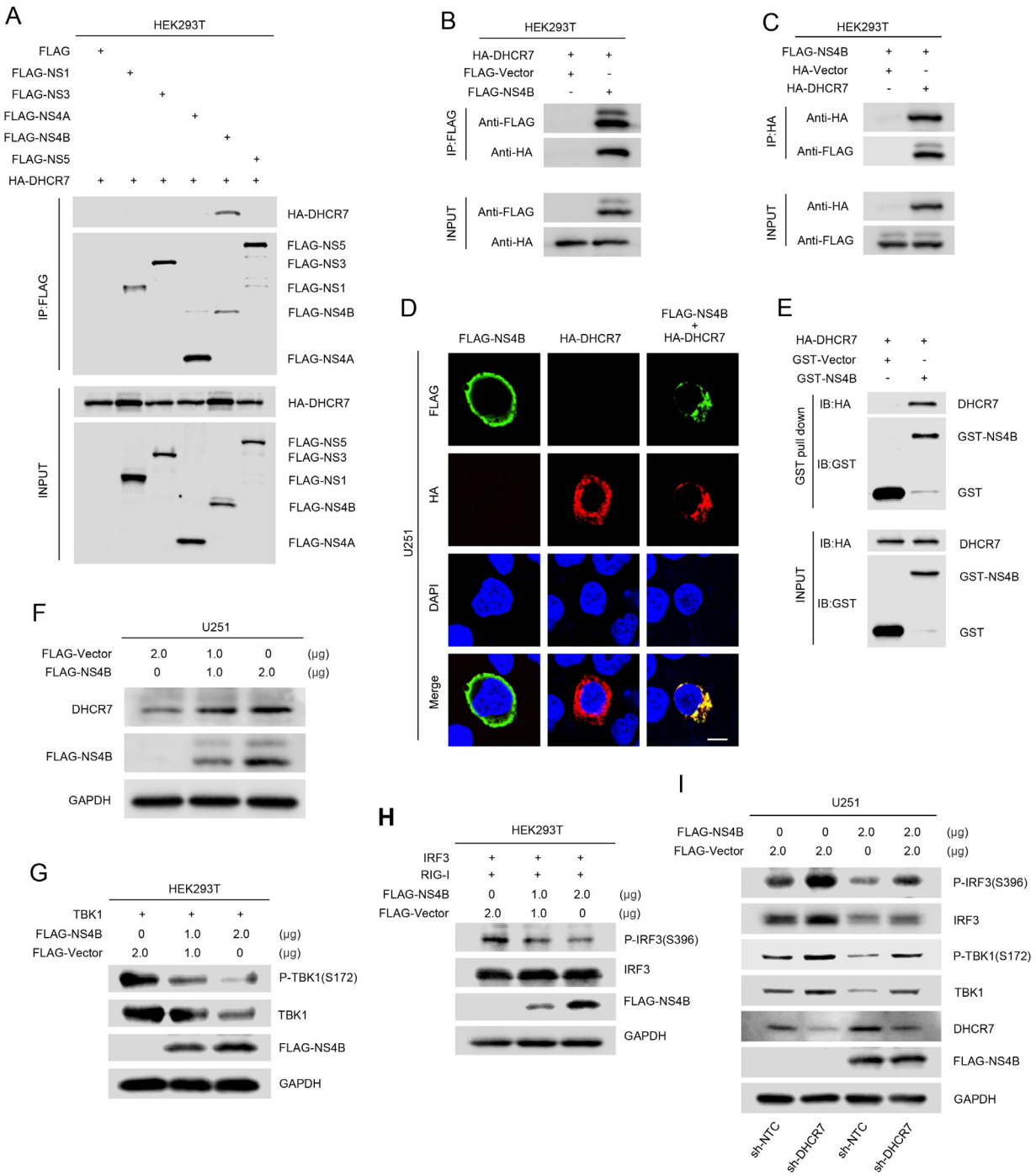

Fig. 6. ZIKV NS4B interacts with DHCR7 to inhibit TBK1 and IRF3 phosphorylation. **A** HEK293T cells were co-transfected with plasmids encoding HA-DHCR7, and plasmids encoding ZIKV non-structural proteins (FLAG-NS1, FLAG-NS3, FLAG-NS4A, FLAG-NS4B, and FLAG-NS5) or empty control plasmid for 30 h. The cell lysates were immunoprecipitated with anti-Flag antibody, and then analyzed by immunoblotting with indicated antibodies. **B, C** HEK293T cells were co-transfected with plasmids encoding HA-DHCR7, plasmids encoding FLAG-NS4B or empty control plasmid for 30 h. The cell lysates were immunoprecipitated with anti-HA antibody (**B**) or anti-FLAG antibody (**C**), and then analyzed by immunoblotting with indicated antibodies. **D** U251 cells were transfected with FLAG-NS4B plasmid together with plasmids encoding with HA-DHCR7. The localization of FLAG-NS4B (green), HA-DHCR7 (red), nucleus marker DAPI (blue), and merge were analyzed with confocal microscopy. Scale bar = 10 μm. **E** Cell lysates from HEK293T cells transfected with HA-DHCR7 were incubated with GST protein or GST-NS4B protein which was incubated with glutathione-Sepharose beads. Mixtures were detected by Western blot with anti-HA and anti-GST antibody (top). Lysates from transfected HEK293T cells and the purified proteins were a detected by Western blot with anti-HA and anti-GST antibody (bottom). **F** U251 cells were transfected with plasmid encoding FLAG-NS4B (0, 1, 2 μg). The relative protein levels of DHCR7, FLAG-NS4B and GAPDH were detected by Western blot. **G, H** HEK293T cells were co-transfected with NS4B-expressing plasmid or empty vector, together with TBK1-coding plasmid (**F**), IRF3-expressing plasmid and plasmids encoding RIG-I (**G**). Cells were harvested at 24 h post-transfection and subjected to Western blot with indicated antibodies [anti-TBK1, anti-P-TBK1(S172), anti-IRF3, anti-P-IRF3(S396), anti-FLAG, and anti-GAPDH]. **I** DHCR7-silencing U251 (sh-DHCR7) and sh-NTC U251 cells were transfected with NS4B-expressing plasmid or empty vector. Cells were harvested at 6 h post-transfection and subjected to Western blot with indicated antibodies [anti-TBK1, anti-P-TBK1(S172), anti-IRF3, anti-P-IRF3(S396), anti-FLAG, and anti-GAPDH]. Data are representative of three independent experiments.

5. Conclusions

In summary, previous study revealed that cholesterol metabolism enzyme DHCR7 involved in innate immune response against various viral infections. Our study has presented that ZIKV NS4B interacted with DHCR7 and induced DHCR7 expression. The increased DHCR7 greatly inhibits TBK1 and IRF3 activation and results in reduced IFN-β and ISGs productions, which thus facilitates ZIKV infection in glial cells. These findings have uncovered a novel viral immune escaping mechanism that ZIKV overcomes immune response by directly targeting on DHCR7 with NS4B.

Data availability

All the data generated during the current study are included in the manuscript.

Ethics statement

This article does not contain any studies with human or animal subjects performed by any of the authors.

Author contributions

Weijie Chen: conceptualization, data curation, formal analysis, investigation, methodology, validation, visualization, writing–original draft preparation, writing–review and editing. Yukun Li: investigation, methodology, validation, visualization. Xiuling Yu: investigation, methodology, validation, visualization. Zhenwei Wang: data curation, methodology, visualization. Wenbiao Wang: data curation, investigation, methodology. Menglan Rao: investigation, methodology, supervision, visualization. Yongkui Li: resources, validation. Zhen Luo: resources, validation. Qiwei Zhang: resources, validation, writing–review and editing. Jinbiao Liu: conceptualization, formal analysis, funding acquisition, project administration, supervision, writing–original draft preparation, writing–review and editing. Jianguo Wu: conceptualization, funding acquisition, project administration, resources, supervision, visualization, writing–review and editing.

Conflict of Interest

The authors declare no conflict of interest.

Acknowledgements

This work was supported by the National Natural Science Foundation of China (81730061, 81802008) and the Guangdong Basic and Applied Basic Research Foundation (2021A1515011272).

Appendix A. Supplementary data

Supplementary data to this article can be found online at https://doi.org/10.1016/j.virs.2022.09.009.

References

Akula, M.K., Shi, M., Jiang, Z., Foster, C.E., Miao, D., Li, A.S., Zhang, X., Gavin, R.M., Forde, S.D., Germain, G., Carpenter, S., Rosadini, C.V., Gritsman, K., Chae, J.J., Hampton, R., Silverman, N., Gravallese, E.M., Kagan, J.C., Fitzgerald, K.A., Kastner, D.L., Golenbock, D.T., Bergo, M.O., Wang, D., 2016. Control of the innate immune response by the mevalonate pathway. Nat. Immunol. 17, 922–929.

Berthoux, L., 2020. The restrictome of flaviviruses. Virol. Sin. 35, 363–377.

Blanc, M., Hsieh, W.Y., Robertson, K.A., Kropp, K.A., Forster, T., Shui, G., Lacaze, P., Watterson, S., Griffiths, S.J., Spann, N.J., Meljon, A., Talbot, S., Krishnan, K., Covey, D.F., Wenk, M.R., Craigon, M., Ruzsics, Z., Haas, J., Angulo, A., Griffiths, W.J., Glass, C.K., Wang, Y., Ghazal, P., 2013. The transcription factor STAT-1 couples macrophage synthesis of 25-hydroxycholesterol to the interferon antiviral response. Immunity 38, 106–118.

Cao-Lormeau, V.-M., Blake, A., Mons, S., Lastère, S., Roche, C., Vanhomwegen, J., Dub, T., Baudouin, L., Teissier, A., Larre, P., Vial, A.-L., Decam, C., Choumet, V., Halstead, S.K., Willison, H.J., Musset, L., Manuguerra, J.-C., Despres, P., Fournier, E., Mallet, H.-P., Musso, D., Fontanet, A., Neil, J., Ghawché, F., 2016. Guillain-Barré Syndrome outbreak associated with Zika virus infection in French Polynesia: a case-control study. Lancet 387, 1531–1539.

Chazal, M., Beauclair, G., Gracias, S., Najburg, V., Simon-Loriere, E., Tangy, F., Komarova, A.V., Jouvenet, N., 2018. RIG-I recognizes the 5' region of dengue and Zika virus genomes. Cell Rep. 24, 320–328.

Chen, Q., Gouilly, J., Ferrat, Y.J., Espino, A., Glaziou, Q., Cartron, G., El Costa, H., Al-Daccak, R., Jabrane-Ferrat, N., 2020. Metabolic reprogramming by Zika virus provokes inflammation in human placenta. Nat. Commun. 11, 2967.

Dang, E.V., McDonald, J.G., Russell, D.W., Cyster, J.G., 2017. Oxysterol restraint of cholesterol synthesis prevents AIM2 inflammasome activation. Cell 171, 1057–1071 e1011.

Ding, Q., Cao, X., Lu, J., Huang, B., Liu, Y.J., Kato, N., Shu, H.B., Zhong, J., 2013. Hepatitis C virus NS4B blocks the interaction of STING and TBK1 to evade host innate immunity. J. Hepatol. 59, 52–58.

Fanunza, E., Grandi, N., Quartu, M., Carletti, F., Ermellino, L., Milia, J., Corona, A., Capobianchi, M.R., Ippolito, G., Tramontano, E., 2021. INMI1 Zika virus NS4B antagonizes the interferon signaling by suppressing STAT1 phosphorylation. Viruses 13, 2448.

Fitzgerald, K.A., McWhirter, S.M., Faia, K.L., Rowe, D.C., Latz, E., Golenbock, D.T., Coyle, A.J., Liao, S.M., Maniatis, T., 2003. IKKε and TBK1 are essential components of the IRF3 signaling pathway. Nat. Immunol. 4, 491–496.

Fitzky, B.U., Witsch-Baumgartner, M., Erdel, M., Lee, J.N., Paik, Y.-K., Glossmann, H., Utermann, G., Moebius, F.F., 1998. Mutations in the Δ7-sterol reductase gene in patients with the Smith–Lemli–Opitz syndrome. Proc. Natl. Acad. Sci. U.S.A. 95, 8181–8186.

Gorman, M.J., Caine, E.A., Zaitsev, K., Begley, M.C., Weger-Lucarelli, J., Uccellini, M.B., Tripathi, S., Morrison, J., Yount, B.L., Dinnon 3rd, K.H., Ruckert, C., Young, M.C., Zhu, Z., Robertson, S.J., McNally, K.L., Ye, J., Cao, B., Mysorekar, I.U., Ebel, G.D., Baric, R.S., Best, S.M., Artyomov, M.N., Garcia-Sastre, A., Diamond, M.S., 2018. An immunocompetent mouse model of Zika virus infection. Cell Host Microbe 23, 672–685.e6.

Grant, A., Ponia, S.S., Tripathi, S., Balasubramaniam, V., Miorin, L., Sourisseau, M., Schwarz, M.C., Sanchez-Seco, M.P., Evans, M.J., Best, S.M., Garcia-Sastre, A., 2016. Zika virus targets human STAT2 to inhibit type I interferon signaling. Cell Host Microbe 19, 882–890.

Hertzog, J., Dias Junior, A.G., Rigby, R.E., Donald, C.L., Mayer, A., Sezgin, E., Song, C., Jin, B., Hublitz, P., Eggeling, C., Kohl, A., Rehwinkel, J., 2018. Infection with a Brazilian isolate of Zika virus generates RIG-I stimulatory RNA and the viral NS5 protein blocks type I IFN induction and signaling. Eur. J. Immunol. 48, 1120–1136.

Horlick, L., 1966. Effect of a new inhibitor of cholesterol biosynthesis (AY 9944) on serum and tissue sterols in the rat. J. Lipid Res. 7, 116–121.

Ikonen, E., 2008. Cellular cholesterol trafficking and compartmentalization. Nat. Rev. Mol. Cell Biol. 9, 125–138.

Kato, H., Takeuchi, O., Sato, S., Yoneyama, M., Yamamoto, M., Matsui, K., Uematsu, S., Jung, A., Kawai, T., Ishii, K.J., Yamaguchi, O., Otsu, K., Tsujimura, T., Koh, C.S., Reis e Sousa, C., Matsuura, Y., Fujita, T., Akira, S., 2006. Differential roles of MDA5 and RIG-I helicases in the recognition of RNA viruses. Nature 441, 101–105.

Kuan, V., Martineau, A.R., Griffiths, C.J., Hyppönen, E., Walton, R., 2013. DHCR7 mutations linked to higher vitamin D status allowed early human migration to northern latitudes. BMC Evol. Biol. 13, 144.

Kumar, A., Hou, S., Airo, A.M., Limonta, D., Mancinelli, V., Branton, W., Power, C., Hobman, T.C., 2016. Zika virus inhibits type-I interferon production and downstream signaling. EMBO Rep. 17, 1766–1775.

Lazear, H.M., Govero, J., Smith, A.M., Platt, D.J., Fernandez, E., Miner, J.J., Diamond, M.S., 2016. A mouse model of Zika virus pathogenesis. Cell Host Microbe 19, 720–730.

Lee, L.J., Komarasamy, T.V., Adnan, N.A.A., James, W., Rmt Balasubramaniam, V., 2021. Hide and seek: the interplay between Zika virus and the host immune response. Front. Immunol. 12, 750365.

Leier, H.C., Weinstein, J.B., Kyle, J.E., Lee, J.Y., Bramer, L.M., Stratton, K.G., Kempthorne, D., Navratil, A.R., Tafesse, E.G., Hornemann, T., Messer, W.B., Dennis, E.A., Metz, T.O., Barklis, E., Tafesse, F.G., 2020. A global lipid map defines a network essential for Zika virus replication. Nat. Commun. 11, 3652.

Li, A., Wang, W., Wang, Y., Chen, K., Xiao, F., Hu, D., Hui, L., Liu, W., Feng, Y., Li, G., Tan, Q., Liu, Y., Wu, K., Wu, J., 2020. NS5 conservative site is required for Zika virus to restrict the RIG-I signaling. Front. Immunol. 11, 51.

Li, C., Deng, Y.Q., Wang, S., Ma, F., Aliyari, R., Huang, X.Y., Zhang, N.N., Watanabe, M., Dong, H.L., Liu, P., Li, X.F., Ye, Q., Tian, M., Hong, S., Fan, J., Zhao, H., Li, L., Vishlaghi, N., Buth, J.E., Au, C., Liu, Y., Lu, N., Du, P., Qin, F.X., Zhang, B., Gong, D., Dai, X., Sun, R., Novitch, B.G., Xu, Z., Qin, C.F., Cheng, G., 2017. 25-Hydroxycholesterol protects host against Zika virus infection and its associated microcephaly in a mouse model. Immunity 46, 446–456.

Liu, C.I., Liu, G.Y., Song, Y., Yin, F., Hensler, M.E., Jeng, W.Y., Nizet, V., Wang, A.H., Oldfield, E., 2008. A cholesterol biosynthesis inhibitor blocks Staphylococcus aureus virulence. Science 319, 1391–1394.

Liu, S.Y., Aliyari, R., Chikere, K., Li, G., Marsden, M.D., Smith, J.K., Pernet, O., Guo, H., Nusbaum, R., Zack, J.A., Freiberg, A.N., Su, L., Lee, B., Cheng, G., 2013. Interferon-inducible cholesterol-25-hydroxylase broadly inhibits viral entry by production of 25-hydroxycholesterol. Immunity 38, 92–105.

Luo, J., Yang, H., Song, B.L., 2020. Mechanisms and regulation of cholesterol homeostasis. Nat. Rev. Mol. Cell Biol. 21, 225–245.

Luu, W., Hart-Smith, G., Sharpe, L.J., Brown, A.J., 2015. The terminal enzymes of cholesterol synthesis, DHCR24 and DHCR7, interact physically and functionally. J. Lipid Res. 56, 888–897.
Ma, J., Ketkar, H., Geng, T., Lo, E., Wang, L., Xi, J., Sun, Q., Zhu, Z., Cui, Y., Yang, L., Wang, P., 2018. Zika virus non-structural protein 4A blocks the RLR-MAVS signaling. Front. Microbiol. 9, 1350.
Moebius, F.F., Fitzky, B.U., Lee, J.N., Paik, Y.K., Glossmann, H., 1998. Molecular cloning and expression of the human delta7-sterol reductase. Proc. Natl. Acad. Sci. U.S.A. 95, 1899–1902.
Munoz-Jordan, J.L., Laurent-Rolle, M., Ashour, J., Martinez-Sobrido, L., Ashok, M., Lipkin, W.I., Garcia-Sastre, A., 2005. Inhibition of alpha/beta interferon signaling by the NS4B protein of flaviviruses. J. Virol. 79, 8004–8013.
Munoz-Jordan, J.L., Sanchez-Burgos, G.G., Laurent-Rolle, M., Garcia-Sastre, A., 2003. Inhibition of interferon signaling by dengue virus. Proc. Natl. Acad. Sci. U.S.A. 100, 14333–14338.
Petersen, J., Drake, M.J., Bruce, E.A., Riblett, A.M., Didigu, C.A., Wilen, C.B., Malani, N., Male, F., Lee, F.H., Bushman, F.D., Cherry, S., Doms, R.W., Bates, P., Briley Jr., K., 2014. The major cellular sterol regulatory pathway is required for Andes virus infection. PLoS Pathog. 10, e1003911.
Pierson, T.C., Diamond, M.S., 2020. The continued threat of emerging flaviviruses. Nat. Microbiol. 5, 796–812.
Prabhu, A.V., Luu, W., Li, D., Sharpe, L.J., Brown, A.J., 2016a. DHCR7: a vital enzyme switch between cholesterol and vitamin D production. Prog. Lipid Res. 64, 138–151.
Prabhu, A.V., Luu, W., Sharpe, L.J., Brown, A.J., 2016b. Cholesterol-mediated degradation of 7-dehydrocholesterol reductase switches the balance from cholesterol to vitamin D synthesis. J. Biol. Chem. 291, 8363–8373.
Randall, G., 2018. Lipid droplet metabolism during dengue virus infection. Trends Microbiol. 26, 640–642.
Rasmussen, S.A., Jamieson, D.J., Honein, M.A., Petersen, L.R., 2016. Zika virus and birth defects–reviewing the evidence for causality. N. Engl. J. Med. 374, 1981–1987.
Reboldi, A., Dang, E.V., McDonald, J.G., Liang, G., Russell, D.W., Cyster, J.G., 2014. Inflammation. 25-Hydroxycholesterol suppresses interleukin-1-driven inflammation downstream of type I interferon. Science 345, 679–684.
Riedl, W., Acharya, D., Lee, J.H., Liu, G., Serman, T., Chiang, C., Chan, Y.K., Diamond, M.S., Gack, M.U., 2019. Zika virus NS3 mimics a cellular 14-3-3-binding motif to antagonize RIG-I- and MDA5-mediated innate immunity. Cell Host Microbe 26, 493–503 e496.
Rodgers, M.A., Villareal, V.A., Schaefer, E.A., Peng, L.F., Corey, K.E., Chung, R.T., Yang, P.L., 2012. Lipid metabolite profiling identifies desmosterol metabolism as a new antiviral target for hepatitis C virus. J. Am. Chem. Soc. 134, 6896–6899.
Savidis, G., Perreira, J.M., Portmann, J.M., Meraner, P., Guo, Z., Green, S., Brass, A.L., 2016. The IFITMs inhibit Zika virus replication. Cell Rep. 15, 2323–2330.
Schneider, W.M., Chevillotte, M.D., Rice, C.M., 2014. Interferon-stimulated genes: a complex web of host defenses. Annu. Rev. Immunol. 32, 513–545.
Shan, Y., Tong, Z., Jinzhu, M., Yu, L., Zecai, Z., Chenhua, W., Wenjing, H., Siyu, L., Nannan, C., Siyu, S., Tongtong, B., Jiang, H., Biaohui, B., Xin, J., Yulong, Z., Zhanbo, Z., 2021. Bovine viral diarrhea virus NS4B protein interacts with 2CARD of MDA5 domain and negatively regulates the RLR-mediated IFN-β production. Virus Res. 302, 198471.
Shim, Y.-H., Bae, S.-H., Kim, J.-H., Kim, K.-R., Kim, C.J., Paik, Y.-K., 2004. A novel mutation of the human 7-dehydrocholesterol reductase gene reduces enzyme activity in patients with holoprosencephaly. Biochem. Biophys. Res. Commun. 315, 219–223.
Wang, Z., Wang, P., An, J., 2016. Zika virus and Zika fever. Virol. Sin. 31, 103–109.
Witsch-Baumgartner, M., Fitzky, B.U., Ogorelkova, M., Kraft, H.G., Moebius, F.F., Glossmann, H., Seedorf, U., Gillessen-Kaesbach, G., Hoffmann, G.F., Clayton, P., Kelley, R.I., Utermann, G., 2000. Mutational spectrum in the Δ7-sterol reductase gene and genotype-phenotype correlation in 84 patients with smith-lemli-opitz syndrome. Am. J. Hum. Genet. 66, 402–412.
Xia, H., Luo, H., Shan, C., Muruato, A.E., Nunes, B.T.D., Medeiros, D.B.A., Zou, J., Xie, X., Giraldo, M.I., Vasconcelos, P.F.C., Weaver, S.C., Wang, T., Rajsbaum, R., Shi, P.Y., 2018. An evolutionary NS1 mutation enhances Zika virus evasion of host interferon induction. Nat. Commun. 9, 414.
Xiao, J., Li, W., Zheng, X., Qi, L., Wang, H., Zhang, C., Wan, X., Zheng, Y., Zhong, R., Zhou, X., Lu, Y., Li, Z., Qiu, Y., Liu, C., Zhang, F., Zhang, Y., Xu, X., Yang, Z., Chen, H., Zhai, Q., Wei, B., Wang, H., 2020. Targeting 7-dehydrocholesterol reductase integrates cholesterol metabolism and IRF3 activation to eliminate infection. Immunity 52, 109–122 e106.
Xu, L., Liu, W., Sheflin, L.G., Fliesler, S.J., Porter, N.A., 2011. Novel oxysterols observed in tissues and fluids of AY9944-treated rats: a model for Smith-Lemli-Opitz syndrome. J. Lipid Res. 52, 1810–1820.
Yi, G., Wen, Y., Shu, C., Han, Q., Konan, K.V., Li, P., Kao, C.C., Simon, A., 2016. Hepatitis C virus NS4B can suppress STING accumulation to evade innate immune responses. J. Virol. 90, 254–265.
York, A.G., Williams, K.J., Argus, J.P., Zhou, Q.D., Brar, G., Vergnes, L., Gray, E.E., Zhen, A., Wu, N.C., Yamada, D.H., Cunningham, C.R., Tarling, E.J., Wilks, M.Q., Casero, D., Gray, D.H., Yu, A.K., Wang, E.S., Brooks, D.G., Sun, R., Kitchen, S.G., Wu, T.T., Reue, K., Stetson, D.B., Bensinger, S.J., 2015. Limiting cholesterol biosynthetic flux spontaneously engages type I IFN signaling. Cell 163, 1716–1729.
Zhang, W., Zeng, M., Jiang, B., Lu, T., Guo, J., Hu, T., Wang, M., Jia, R., Zhu, D., Liu, M., Zhao, X., Yang, Q., Wu, Y., Zhang, S., Ou, X., Liu, Y., Zhang, L., Yu, Y., Pan, L., Cheng, A., Chen, S., 2021. Amelioration of beta interferon inhibition by NS4B contributes to attenuating tembusu virus virulence in ducks. Front. Immunol. 12, 671471.
Zheng, Y., Liu, Q., Wu, Y., Ma, L., Zhang, Z., Liu, T., Jin, S., She, Y., Li, Y.P., Cui, J., 2018. Zika virus elicits inflammation to evade antiviral response by cleaving cGAS via NS1-caspase-1 axis. EMBO J. 37, e99347.
Zou, J., Xie, X., Lee le, T., Chandrasekaran, R., Reynaud, A., Yap, L., Wang, Q.Y., Dong, H., Kang, C., Yuan, Z., Lescar, J., Shi, P.Y., 2014. Dimerization of flavivirus NS4B protein. J. Virol. 88, 3379–3391.